IEEE Access
Multidisciplinary | Rapid Review | Open Access Journal

Received July 17, 2019, accepted July 25, 2019, date of publication July 30, 2019, date of current version August 15, 2019.

*Digital Object Identifier 10.1109/ACCESS.2019.2931948*

# Error Averaging Effect of Hydrostatic Journal Bearings Considering the Influences of Shaft Rotating Speed and External Load

**YONGTAO ZHANG[1], CHANGHOU LU[2,3,4], HAIXIA ZHAO[1], WEIJIE SHI[1], AND PENG LIANG[5]**

[1]College of Electromechanical Engineering, Qingdao University of Science and Technology, Qingdao 266061, China
[2]School of Mechanical Engineering, Shandong University, Jinan 250061, China
[3]Key Laboratory of High-efficiency and Clean Mechanical Manufacture, Ministry of Education, Shandong University, Jinan 250061, China
[4]National Demonstration Center for Experimental Mechanical Engineering Education, Jinan 250061, China
[5]School of Mechanical and Automotive Engineering, Qingdao University of Technology, Qingdao 266033, China

Corresponding authors: Yongtao Zhang (zhyt@qust.edu.cn) and Changhou Lu (luchh@sdu.edu.cn)

This work was supported by the Department of Science and Technology of Shandong Province under Grant 2017CXGC0803 and Grant 2018GSF117038.

**ABSTRACT** Hydrostatic journal bearings possess superior motion accuracy owing to their error averaging effect and often work under different speeds and external loads in precision applications. This paper researches the error averaging effect of hydrostatic journal bearings considering the influences of shaft rotating speeds and external loads. A new mathematical model is established based on a time division method where the rotational movement of the shaft is divided into many time intervals. The averaging coefficients of hydrostatic journal bearings are analyzed in detail. The results show that the averaging coefficients are affected by the combined effects of rotational speeds, and external loads and wave number of roundness errors. Finally, some useful guidelines are given for the accuracy design of hydrostatic journal bearings.

**INDEX TERMS** Averaging effect, hydrostatic journal bearing, motion error, transient orbit.

## I. INTRODUCTION

Hydrostatic journal bearings are widely applied in precision applications due to their high motion accuracy, low friction, and long life [1]. Radial motion errors of hydrostatic journal bearings are mainly affected by roundness errors of the shaft. By predicting the radial motion errors, some guidelines for the accuracy design of hydrostatic journal bearings can be given.

Many studies have found that the radial motion errors could be smaller than the roundness errors owing to the error averaging effect of fluid film [2]–[4]. Kane et al. [2] experimentally measured the radial motion errors of a hydrostatic bearing. They discovered that the radial motion errors could reach 0.05 $\mu$m under the grinding components with accuracy of only 2.5 $\mu$m, i.e. the motion accuracy increased by 50 times owing to the error averaging effect. By coarsely adjusting the stiffness and finely adjusting the damping of hydrostatic fluid film, Aleyaasin et al. [3] improved the motion accuracy of shaft to 3 $\mu$m under the components with accuracy of 35 $\mu$m. Cappa et al. [4] proposed a numerical air film model for analyzing the effect of various geometric errors on motion accuracy of aerostatic journal bearings. They found that the radial motion accuracy could be improved by adopting more air feedholes. Based on Hertzian contact theory and Runge-Kutta-Fehlberg method, Jang and Jeong [5] studied the influence of wave errors of the bearings on the vibration of the shaft. Zhang et al. [6] researched the influence of manufacturing and assembly errors on motion errors of the shaft in hydrostatic thrust bearings, and verified that the tilt errors of two plates were the main factor in reducing motion accuracy. Zhang et al. [7] proposed an approximate calculation method, for predicting the motion errors of a hydrostatic journal bearing. The structure of six recesses was verified to have higher motion accuracy than the structure of four recesses. Cui et al. [8] adopted the method of computational fluid dynamics and dynamic mesh to investigate running accuracy of an aerostatic spindle under different manufacturing errors. However, a lot of run time was needed for this method.

Some researchers also investigated the error averaging effect in hydrostatic guideways, which belong to the field

The associate editor coordinating the review of this manuscript and approving it for publication was Tao Wang.

of hydrostatic supporting together with hydrostatic bearings. By establishing transfer function in hydrostatic guideways, Shamoto et al. [9] calculated the motion errors of the table and proposed a method of reprocessing guide rail to improve the motion accuracy. Ekinci et al. [10], [11] made a machine error analysis according to causality principle, and analyzed the motion errors of aerostatic guideways depending on the stiffness of aerostatic joint. By averaging fluid film thickness, Xue et al. [12] built an approximate model for analyzing the motion errors of a hydrostatic guideway. Zha et al. studied the motion straightness of hydrostatic guideways under different spacings of oil pad [13] and made an accuracy design according to the relation between motion straightness and geometry error [14]. Qi et al. [15] researched the motion errors of hydrostatic guideways based on three-dimensional profile errors. They found that the profile error in the width directions also affects the motion errors of hydrostatic guideways. Zhang et al. [16], [17] proposed a method of taking hydrostatic lead screws as an especial hydrostatic guideway to research the error averaging effect in hydrostatic lead screws. Zhang et al. [18] established an approximate model based on equivalent fluid film thickness, for studying the motion accuracy of hydrostatic guideways considering the manufacturing errors of both the table and the guide rails. They found that the manufacturing errors of guide rails were the major factor affecting the motion accuracy. He et al. [19] proposed a hierarchical calculation method for obtaining the motion error of the table, in which the motion error was divided into four layers and two adjacent layers were interconnected. By establishing transfer function in aerostatic guideways, Khim et al. [20] investigated the motion errors of an aerostatic guideway in five-degrees-of-freedom. The experiments were conducted using the method of mixed sequential two-probe to validate the theoretical model. Khim et al. [21] adopted a reverse reasoning method to obtain the geometry error of guide rail from the measured motion errors. The guide rail was reprocessed for improving the motion accuracy, in which straightness motion accuracy increases by 1 $\mu$m and the angular motion accuracy increases by 1-2 arcsec. Tang et al. [22] made a comprehensive geometry error analysis for the guide rail surface according to actual manufacturing process, and calculated the motion errors of table based on the fitting expression of the guideway surface. In summary, the mathematical models in above-mentioned reports all depend on static equilibrium, i.e. the shaft or table moves at very low speed.

For high speed condition, Wang et al. [23] proposed a method of simultaneously solving the Reynolds equation of fluid film and the motion equation of the table, for analyzing the influence of the speed of table on the motion errors of hydrostatic guideways. Zha et al. [24] established a run-out error model for numerically calculated the axial run-out error of a hydrostatic thrust bearing under high speed condition. Kirk and Gunter [25] analyzed the transient orbit of shaft in hydrodynamic journal bearings under imbalance loads, steady loads, and periodic loads.

There is rare report on the error averaging effect of hydrostatic journal bearings considering the influences of the rotational speed of the shaft and the external load. However, the hydrostatic journal bearing often runs at different speeds and bears different external loads in precision applications. Hence, this study establishes a new mathematical model where the speed effect and the load effect are taken into consideration, for making a more realistic prediction of the error averaging effect of hydrostatic journal bearings. The rotational movement of the shaft in hydrostatic journal bearings is divided into a time series. At each time step, the time-transient Reynolds equation is solved using finite difference technique, and the motion equation of the shaft is handled by the Euler method. Then the transient orbit of the shaft is obtained and the motion errors of the shaft are investigated under different rotational speeds and external loads. The error averaging effect is analyzed in detail, which provides a useful guidance for the accuracy design of hydrostatic journal bearings.

## II. MATHEMATICAL MODELS

### A. HYDROSTATIC JOURNAL BEARING AND FLUID FILM THICKNESS

Fig. 1(a) shows a typical capillary compensated four-recess hydrostatic journal bearing. The four recesses are labeled as 1, 2, 3, and 4, respectively. The red curve represents the contour of the shaft with roundness errors, and the black circle represents the contour of the shaft without roundness errors. Fig. 1(b) shows the developed view of the bearing surface along the circumferential direction. $\theta$ represents the angular coordinate. The motion accuracy of shaft is mainly affected by the roundness errors of shaft [4], [7]. Thus, this study only considers the roundness errors of the shaft. The roundness errors of bearing are ignored and the inner surface of the bearing surface is regarded as an ideal circle. When an external load $W$ is applied on the shaft with the rotational speed of $\omega$, the shaft center will deviates from the bearing center. The error averaging effect will change with the variation of the external load $W$.

Fig. 2 shows the calculating diagram of the fluid film thickness. The roundness errors of the shaft are the sum of various harmonic waves with different amplitudes, frequencies and phases, which can be formulated using Fourier series. According to the geometric relationship, the fluid film thickness of any point A can be calculated by

$$h = c + x_s \cos\theta + y_s \sin\theta - \sum_{n=1}^{\infty} E_n \cos\left[n\left(\theta - \omega t\right) + \varphi_n\right] \quad (1)$$

where $c$ is the radial clearance, $(x_s, y_s) = (e\cos\phi, e\sin\phi)$ is the coordinate of shaft center $O_s$, $e$ is the eccentricity, $\phi$ is the attitude angle, $E_n$ and $\varphi_n$ are the amplitude and phase for the $n$th term of Fourier series, and $n$ represents the wave number of roundness errors in one circle on the outer cylindrical surface of the shaft. When the shaft has only a certain frequency of the Fourier series, the fluid film

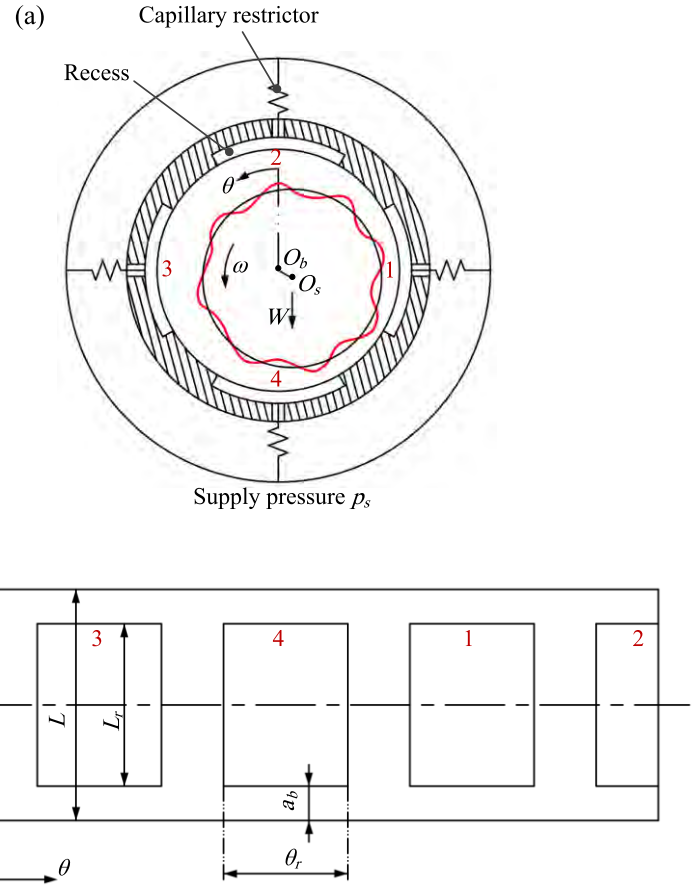


**FIGURE 1.** (a) Capillary compensated four-recess hydrostatic journal bearing and (b) developed view of bearing surface.

thickness is

$$h = c + x_s \cos\theta + y_s \sin\theta - E\cos\left[n\left(\theta - \omega t\right) + \varphi\right] \tag{2}$$

Substituting dimensionless parameters $\bar{h} = h/c$, $\varepsilon = e/c$, $\bar{x}_s = \varepsilon\cos\phi$, $\bar{y}_s = \varepsilon\sin\phi$, and $\bar{E} = E/c$, the dimensionless fluid film thickness is

$$\bar{h} = 1 + \bar{x}_s \cos\theta + \bar{y}_s \sin\theta - \bar{E}\cos\left[n\left(\theta - \omega t\right) + \varphi\right] \tag{3}$$

### B. REYNOLDS EQUATION

The Reynolds equation for the fluid film in the clearance space between the shaft and the bearing is expressed as [26]

$$\frac{1}{r^2}\frac{\partial}{\partial\theta}\left(h^3\frac{\partial p}{\partial\theta}\right) + \frac{\partial}{\partial z}\left(h^3\frac{\partial p}{\partial z}\right) = 6\eta\omega\frac{\partial h}{\partial\theta} + 12\eta\frac{\partial h}{\partial t} \tag{4}$$

where $p$ is fluid film pressure, $r$ is the shaft radius, $z$ is the axial coordinate, $t$ is the time, and $\eta$ is the dynamic viscosity of the lubricant, which is the function of the lubricant temperature $T$, i.e.

$$\eta = \eta_0 e^{-\beta(T - T_0)} \tag{5}$$

where $\eta_0$ is the dynamic viscosity at the lubricant temperature $T_0$, and $\beta$ is the viscosity-temperature index.

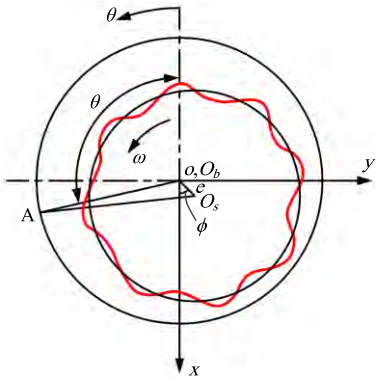


**FIGURE 2.** Calculating diagram of fluid film thickness.

Assuming the input power of oil pump and the friction power are all converted into heat, and the heat is absorbed and taken away by the lubricant, the temperature rise of the lubricant can be expressed as

$$\Delta T = T - T_0 = \frac{P_p + P_f}{c_h \rho Q_s} \tag{6}$$

where $c_h$ is the specific heat capacity of the lubricant, $\rho$ is the density of the lubricant, and $Q_s$ is the total flow. $P_p$ is the input power of oil pump and $P_f$ is the friction power, which

can be written as

$$\begin{cases} P_p = p_s Q_s \\ P_f = F_f v \end{cases} \tag{7}$$

where $p_s$ is the supply pressure, $F_f$ is the frictional force, and $v$ is the velocity on the outer cylinder of the shaft ($v = r\omega$).

Substituting dimensionless parameters $\bar{p} = p/p_s$, $\bar{z} = z/L$, $\Lambda = 6\eta\omega r^2/(p_s c^2)$, and $\tau = \omega t$ into Eq. (4), the dimensionless Reynolds equation can be written as

$$\frac{\partial}{\partial\theta}\left(\bar{h}^3\frac{\partial\bar{p}}{\partial\theta}\right) + \left(\frac{r}{L}\right)^2\frac{\partial}{\partial\bar{z}}\left(\bar{h}^3\frac{\partial\bar{p}}{\partial\bar{z}}\right) = \Lambda\frac{\partial\bar{h}}{\partial\theta} + 2\Lambda\frac{\partial\bar{h}}{\partial\tau} \tag{8}$$

### C. FLOW CONTINUITY EQUATION

The flow continuity equation is [23]

$$Q_{ck} = Q_{ink} + \dot{V}_k + \frac{V_k}{E_l}\frac{\partial p_{rk}}{\partial t} \quad (k = 1, 2, 3, 4) \tag{9}$$

where $Q_{ck}$ is the lubricant flow out the $k$th capillary restrictor, $Q_{ink}$ is the lubricant flow into the $k$th recess land, $p_{rk}$ is the pressure in the $k$th recess, and $V_k$ is the sum of the volume of the $k$th recess $V_{rk}$ and the volume of the $k$th connection channel $V_{ck}$. the connection channel refers to the fluid channel connecting the restrictor and the recess. The several terms in Eq. (9) can be written as [23]

$$\begin{cases} Q_{ck} = \dfrac{\pi d_c^4\,(p_s - p_{rk})}{128\eta l_c} \\ Q_{ink} = \displaystyle\int_{\Gamma_1}\left(\frac{h_k^3}{12\eta r}\frac{\partial p_k}{\partial\theta} - \frac{r\omega h_k}{2}\right)dz \\ \qquad + \displaystyle\int_{\Gamma_2}\left(-\frac{h_k^3}{12\eta r}\frac{\partial p_k}{\partial\theta} + \frac{r\omega h_k}{2}\right)dz \\ + \displaystyle\int_{\Gamma_3}\left(\frac{h_k^3}{12\eta}\frac{\partial p_k}{\partial z}\right)rd\theta + \int_{\Gamma_4}\left(-\frac{h_k^3}{12\eta}\frac{\partial p_k}{\partial z}\right)rd\theta \\ \dot{V}_k = \dot{V}_{rk} + \dot{V}_{ck} = \displaystyle\iint_{Recess}\frac{\partial h_k}{\partial t}rd\theta dz + \frac{V_{ck}}{E_c}\frac{\partial p_{rk}}{\partial t} \end{cases} \tag{10}$$

where $l_c$ and $d_c$ are the length and diameter of the capillary restrictor, respectively, and $E_c$ is the bulk modulus of the connection channel. Because the connection channel, manufactured within the bearing, is rigid ($E_c = \infty$), the last term $(V_{ck}/E_c)\,(\partial p_{rk}/\partial t)$ in the expression of $\dot{V}_k$ equals zero.

Substituting dimensionless parameters $\bar{Q}_{ck} = \left(12\eta/(p_s c^3)\right)Q_{ck}$, $\bar{Q}_{ink} = \left(12\eta/(p_s c^3)\right)Q_{ink}$, $\bar{C}_{sr} = 3\pi d_c^4/\left(32c^3 l_c\right)$, $\bar{p}_{rk} = p_{rk}/p_s$, and $\bar{\dot{V}}_k = \dot{V}_k/(cr\omega L)$. The dimensionless form of Eq. (10) can be expressed as

$$\begin{cases} \bar{Q}_{ck} = \bar{C}_{sr}\,(1 - \bar{p}_{rk}) \\ \bar{Q}_{ink} = \dfrac{B}{L_e/4}\displaystyle\int_{\Gamma_1}\left(\bar{h}_k^3\frac{\partial\bar{p}_k}{\partial\bar{x}_{nk}} + \Lambda\bar{h}_k\right)d\bar{y}_{nk} \\ + \dfrac{B}{L_e/4}\displaystyle\int_{\Gamma_2}\left(-\bar{h}_k^3\frac{\partial\bar{p}_k}{\partial\bar{x}_{nk}} - \Lambda\bar{h}_k\right)d\bar{y}_{nk} \\ + \dfrac{L_e/4}{B}\displaystyle\int_{\Gamma_3}\left(\bar{h}_k^3\frac{\partial\bar{p}_k}{\partial\bar{y}_{nk}}\right)d\bar{x}_{nk} + \frac{L_e/4}{B}\int_{\Gamma_4}\left(-\bar{h}_k^3\frac{\partial\bar{p}_k}{\partial\bar{y}_{nk}}\right)d\bar{x}_{nk} \\ \bar{\dot{V}}_k = \displaystyle\iint_{Recess}\frac{\partial\bar{h}_k}{\partial\tau}d\bar{x}_{nk}d\bar{y}_{nk} \end{cases} \tag{11}$$

The dimensionless form of the flow continuity equation can be expressed as

$$\bar{Q}_{ck} = \bar{Q}_{ink} + \frac{2\Lambda L}{r}\bar{\dot{V}}_k + \Lambda_2\frac{\partial\bar{p}_{rk}}{\partial\tau} \quad (k = 1, 2, 3, 4) \tag{12}$$

where $\Lambda_2 = 12\eta\omega V_k/\left(c^3 E_l\right)$.

### D. BOUNDARY CONDITIONS

(1) The pressure of the nodes on the end face of the bearing equals zero.

(2) The nodes in the recess equals have equal pressure.

(3) The Eq. (12) is satisfied on the boundary of recess.

(4) Reynolds boundary condition ($p = \partial p/\partial\theta = 0$) is satisfied on the cavitation region.

### E. FLUID FILM FORCE

The dimensionless form of the fluid film force in the $x$ and $y$ directions is

$$\begin{cases} \bar{F}_x = \dfrac{F_x}{p_s L r} = \displaystyle\int_0^1\int_0^{\bar{L}}\bar{p}\cos\theta d\theta d\bar{z} \\ \bar{F}_y = \dfrac{F_y}{p_s L r} = \displaystyle\int_0^1\int_0^{\bar{L}}\bar{p}\sin\theta d\theta d\bar{z} \end{cases} \tag{13}$$

The dimensionless form of the frictional force is

$$\bar{F}_f = \frac{h_0}{\eta_0 L r v}F_f = \int_0^1\int_0^{\bar{L}}\frac{1}{\bar{h}}d\theta d\bar{z} \tag{14}$$

### F. MOTION EQUATION OF THE SHAFT AND EULER EQUATION

The motion equation of the shaft is expressed as

$$\begin{cases} M\ddot{x}_s = F_x(\omega t) + W_x + Mg \\ M\ddot{y}_s = F_y(\omega t) + W_y \end{cases} \tag{15}$$

where $M$ is the mass of the shaft. $\ddot{x}_s$ and $\ddot{y}_s$ are the acceleration of shaft, respectively. $W_x$ and $W_y$ are the external load applied on shaft. Dividing Eq. (15) by $Mc\omega^2$ and substituting dimensionless parameters $\bar{\ddot{x}}_s = \ddot{x}_s/(c\omega^2)$, $\bar{\ddot{y}}_s = \ddot{y}_s/(c\omega^2)$, $\Lambda_3 = p_s Lr/(Mc\omega^2)$, $\Lambda_4 = g/(c\omega^2)$, $\overline{W}_x = W_x/(p_s Lr)$, and $\overline{W}_y = W_y/(p_s Lr)$, the dimensionless form of the motion equation is

$$\begin{cases} \bar{\ddot{x}}_s = \Lambda_3\left(\bar{F}_x(\tau) + \overline{W}_x\right) + \Lambda_4 \\ \bar{\ddot{y}}_s = \Lambda_3\left(\bar{F}_x(\tau) + \overline{W}_y\right) \end{cases} \tag{16}$$

Without loss of generality, it can be obtained that $\overline{W}_x = \overline{W}$ and $\overline{W}_y = 0$ by assuming the external load is vertical downward.

The Euler equation under constant time interval $\Delta\tau$ can be written as

$$\begin{cases} \bar{\dot{x}}_s(\tau + \Delta\tau) = \bar{\dot{x}}_s(\tau) + \bar{\ddot{x}}_s(\tau)\,\Delta\tau \\ \bar{x}_s(\tau + \Delta\tau) = \bar{x}_s(\tau) + \bar{\dot{x}}_s(\tau + \Delta\tau)\,\Delta\tau \end{cases} \tag{17}$$

$$\begin{cases} \bar{\dot{y}}_s(\tau + \Delta\tau) = \bar{\dot{y}}_s(\tau) + \bar{\ddot{y}}_s(\tau)\,\Delta\tau \\ \bar{y}_s(\tau + \Delta\tau) = \bar{y}_s(\tau) + \bar{\dot{y}}_s(\tau + \Delta\tau)\,\Delta\tau \end{cases} \tag{18}$$

### G. AVERAGING COEFFICIENT

In order to quantitatively measure the error averaging effect and considering the radial motion of the shaft has directivity, the averaging coefficients $\delta_x$ and $\delta_y$ are defined as the ratio of the amplitude of the motion orbits of the shaft $E_x$ (in the $x$ direction) and $E_y$ (in the $y$ direction) to the amplitude of the roundness errors $E$, i.e. $\delta_x = E_x/E$ and $\delta_y = E_y/E$. The smaller the averaging coefficient is, the smaller radial motion errors the shaft can obtain, and the higher the motion accuracy is.

### H. SOLUTION SCHEME

Under the condition that the speed effect is taken into consideration, the transient orbit of the shaft should be solved, which demonstrates the radial motion errors. The rotational movement of shaft is divided into many time intervals. The time-transient Reynolds equation and the flow continuity equation are solved using the finite difference technique at each time step, and the motion equation of the shaft is handled by the Euler method. After obtaining the transient orbit of the shaft, the averaging coefficients $\delta_x$ and $\delta_y$ can be calculated. The detailed solution procedure of the transient orbit and the averaging coefficients are shown in Fig. 3, in which the dimensionless calculated time of $12\pi$ is set for obtaining transient motion orbit of each situation. The fluid film is divided into 100 grids in radial direction and 180 grids in circumferential direction in the finite difference technique.

## III. RESULTS AND DISCUSSIONS

The numerical calculation was validated by comparing the results from the present calculation program with the results in published references, as follows: Firstly, Fig. 4 compares the transient orbits of shaft with the reference [25], in which the shaft is supported by fluid-film journal bearing. The two results have a good consistency, which validates the correctness of the calculation of the transient orbit. Secondly, the motion errors of the hydrostatic table can be calculated using the calculation program in this study, because the hydrostatic guideway belongs to the field of hydrostatic supporting together with hydrostatic bearings. Fig. 5 compares the motion error of the hydrostatic guideway with experimental data in the reference [9]. It can be seen from Fig. 5 that the simulation results from the present calculation program show good consistency with the results in the reference [9], which validates the correctness of the calculation method of the motion errors, as well as the averaging coefficients.

The parameters of the multi-recess hydrostatic journal bearing are listed in Table 1, which takes the same values as the reference [26] and are obtained from a general design process of hydrostatic journal bearings according to the handbook of mechanical design.

### A. AVERAGING COEFFICIENT UNDER DIFFERENT ROTATIONAL SPEEDS AND EXTERNAL LOADS

Figs. 6 and 7 show the variation of the averaging coefficients $\delta_x$ and $\delta_y$ with the wave number $n$ under different rotational speeds $\omega$ and external loads $W$, respectively. The center point $O_s$ is chosen for assessing the radial motion error in this study, because the roundness errors of the shaft are given under the center point $O_s$. When the wave number $n$ equals 1, the averaging coefficients $\delta_x$ and $\delta_y$ equal 1 under rotation center $O_s$ shown in Fig. 8(a), i.e. the amplitude of radial motion error equals that of the harmonic errors of shaft, while the averaging coefficients $\delta_x$ and $\delta_y$ equal 0 under rotation center $O'_s$, i.e. the shaft has no radial motion error because the harmonic components of roundness errors reconstitute a

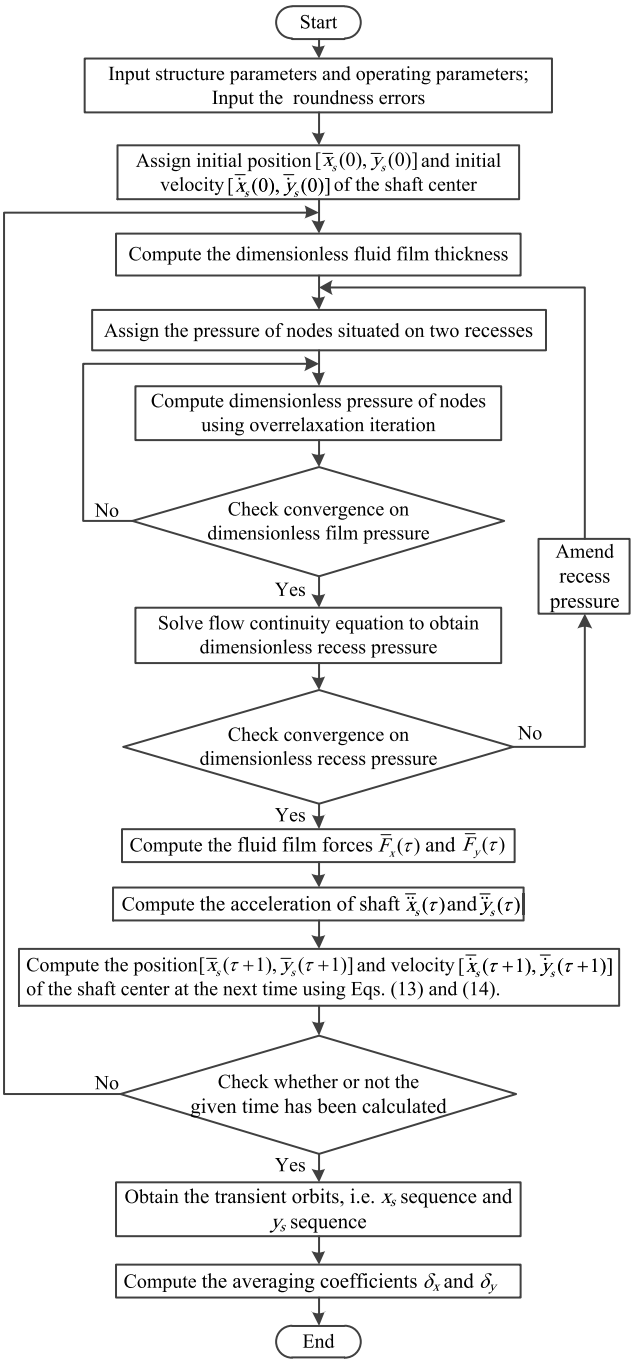


**FIGURE 3. Solution procedure of transient orbits and averaging coefficients.**

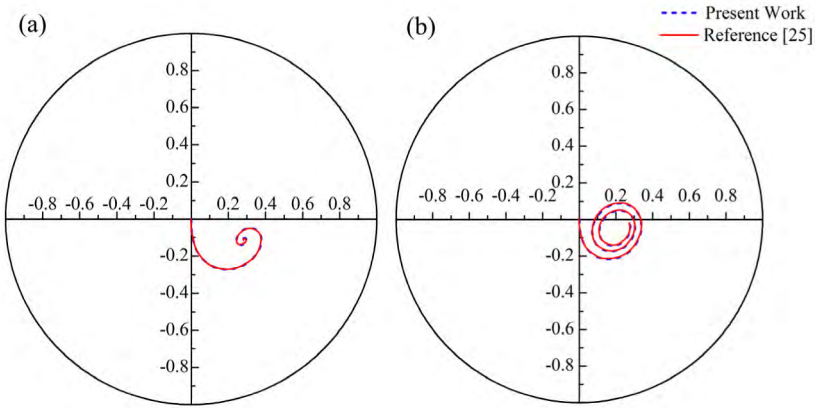


**FIGURE 4.** Transient orbits of shaft under different rotational speeds: (a) $\omega = 4000$ r/min and (b) $\omega = 6500$ r/min.

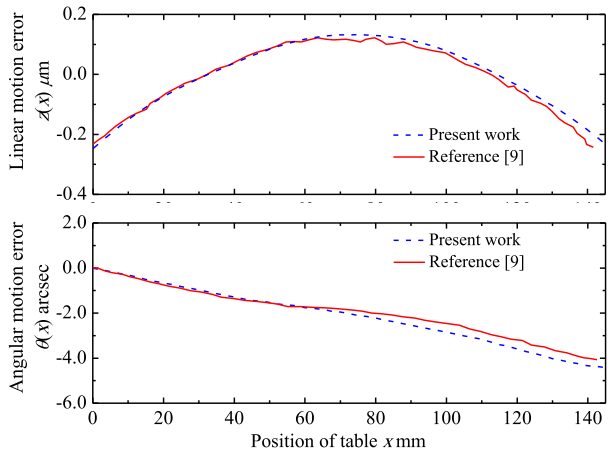


**FIGURE 5.** Motion error of hydrostatic guideway.

**TABLE 1.** Parameters of the multi-recess hydrostatic journal bearing.

| Parameters | Value |
|---|---|
| Bearing length ( $L$ ) | 80 mm |
| Land width in axial direction ( $a_b$ ) | 8 mm |
| Diameter of the shaft ( $D$ ) | 80 mm |
| Mass of the shaft ( $M$ ) | 50 kg |
| Radius clearance ( $c$ ) | 0.025 (0.020, 0.030)mm |
| Rotational speed ( $\omega$ ) | 1000, 2000, 3000 r/min |
| Recess shape | Rectangular |
| Number of recesses | 4 |
| Wrap angle of the recess ( $\theta_r$ ) | 60° |
| Depth of the recess ( $d_r$ ) | 1.5 mm |
| Type of compensating element | Capillary |
| Length of capillary restrictor ( $l_c$ ) | 60 mm |
| Diameter of capillary restrictor ( $d_c$ ) | 0.56 mm |
| Supply pressure ( $p_s$ ) | 2.07 MPa |
| Dynamic viscosity of lubricant at 30 °C ( $\eta_0$ ) | 0.0087 Pa s |
| Specific heat capacity ( $c_h$ ) | 1870 J/(kg °C) |
| Density of lubricant ( $\rho$ ) | 875 kg/m$^3$ |
| Viscosity-temperature index ( $\beta$ ) | 1.78 |
| Connected channel volume ( $V_{ck}$ ) | 4 cm$^3$ |
| Apparent bulk modulus of lubricant ( $E_l$ ) | 1473 MPa |
| Amplitude of roundness error of shaft ( $E$ ) | 1.5 μm |
| Phase of roundness error of shaft ( $\varphi$ ) | 0 |

circle (the shaft has not roundness errors in this situation). In order to get uniform expressions, averaging coefficients in Figs. 6 and 7 are given based on the rotation center of $O_s$ for assessing the radial motion error.

It can be seen from Figs. 6 and 7 that:

(1) When the rotational speed $\omega$ equals 10 r/min and the external load $W$ equals 0 kN (the black lines), the averaging coefficients $\delta_x$ and $\delta_y$ are both equal to zero under the wave number $n$ of 2, 4, 6, 8, 10, ...(equals an even number). This is because the shaft has an even number of lobes, assembling with a bearing with four recesses, which results in the film thickness has the same change in the opposite position. As an example, Fig. 8(b) shows the case where the wave number $n$ equals 2. The change of the fluid film force can be offset and the shaft has no radial motion error. The averaging coefficients $\delta_x$ and $\delta_y$ are not zero under the wave number $n$ of 1, 3, 5, 7, 9, ...(equals an odd number). In this situation, the averaging coefficients $\delta_x$ and $\delta_y$ as a whole have a decreasing trend with the increase of the wave number $n$. Under the wave number $n$ of 3, the averaging coefficients $\delta_x$ and $\delta_y$, having a larger value, equal 0.44 and 0.42, respectively. Fig. 8(c) shows the case where the wave number $n$ equals 3.When the wave number $n$ is larger than 9, the averaging coefficients $\delta_x$ and $\delta_y$ are both smaller than 0.1, i.e. the radial motion error is smaller than $0.1E$.

(2) As shown in Figs. 6(a) and 7(a), with the rotational speed $\omega$ increasing from 0 r/min to 1000 r/min under the external load $W$ of 0 kN (the red lines), the averaging coefficients $\delta_x$ and $\delta_y$ have an obvious decrease, especially for the case where the wave number $n$ equals 3 ($\delta_x$ decreases from 0.44 to 0.12 and $\delta_y$ decreases from 0.42 to 0.12). When the rotational speed $\omega$ remains unchanged, the averaging coefficients $\delta_x$ and $\delta_y$ are gradually increasing with the external load $W$ increasing from 0 kN to 2.5 kN, and 5 kN. This is because with increase in the external load $W$, the eccentricity ratio of the shaft gradually increases, resulting in the enhancement of the hydrodynamic effect, which deteriorates the error averaging effect. Meanwhile, The averaging coefficients $\delta_x$ and $\delta_y$

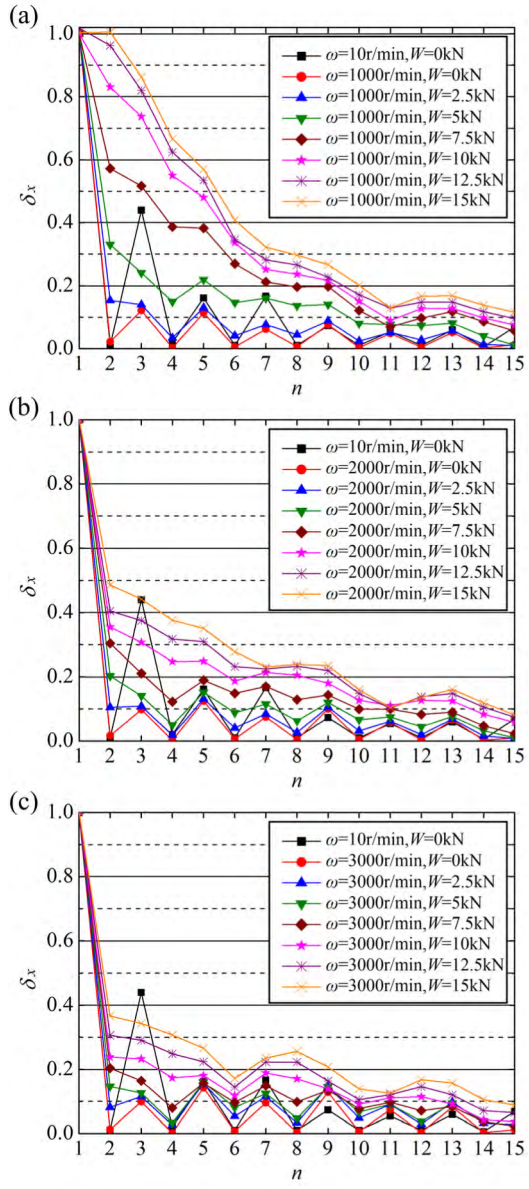


**FIGURE 6.** Averaging coefficients $\delta_x$ for different rotational speeds $\omega$ and external loads $W$: (a) $\omega$ = 1000 r/min, (b) $\omega$ = 2000 r/min, and (c) $\omega$ = 3000 r/min.

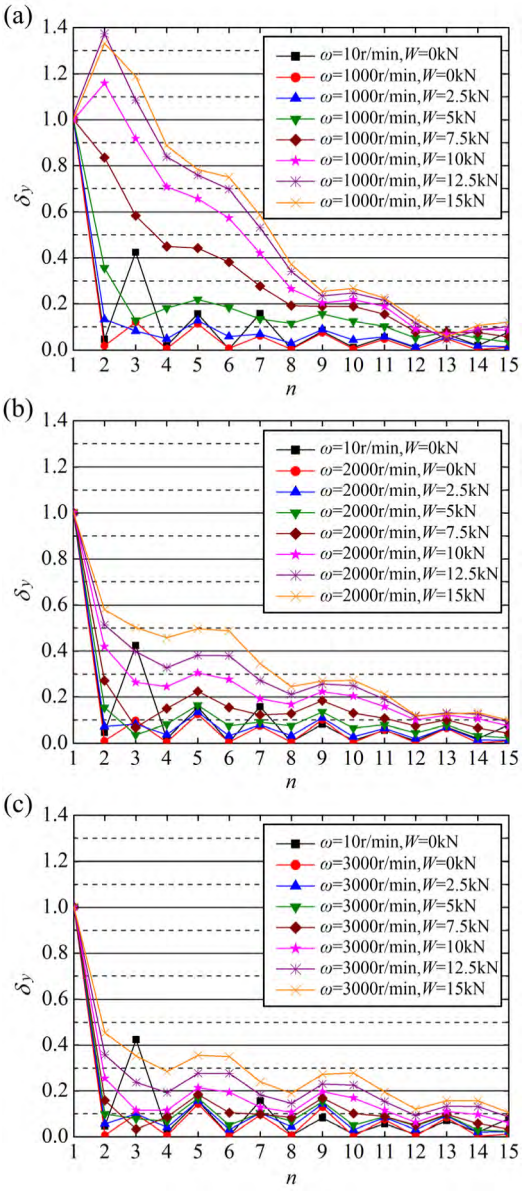


**FIGURE 7.** Averaging coefficients $\delta_y$ for different rotational speeds $\omega$ and external loads $W$: (a) $\omega$ = 1000 r/min, (b) $\omega$ = 2000 r/min, and (c) $\omega$ = 3000 r/min.

become not equal to 0 under the wave number $n$ of 2, 4, 6, 8, 10, ...(equals an even number). With the external load $W$ further increasing from 5 kN to 7.5 kN, 10 kN, 12.5 kN, and 15 kN, the error averaging effect deteriorates significantly, especially for the case where the wave number $n$ is smaller than 7. The averaging coefficient $\delta_y$ is even larger than 1 under the wave number $n$ of 2 and 3. In this situation, the fluid film not only has not error averaging effect, but enlarges the radial motion error.

(3) As shown in Figs. 6(b)-(c) and 7(b)-(c), when the external load $W$ remains unchanged, the averaging coefficients $\delta_x$ and $\delta_y$ have an obvious decrease with the rotational speed $\omega$ increasing from 1000 r/min to 2000 r/min and 3000 r/min. As an example, under the wave number $n$ of 2 and the external load $W$ of 10 kN, relative to the case where the rotational speed $\omega$ of 1000 r/min, the averaging coefficient $\delta_x$ decreases 0.48 (57.30%) for the rotational speed $\omega$ of 2000 r/min and 0.59 (71.23%) for the rotational speed $\omega$ of 3000 r/min, and the averaging coefficient $\delta_y$ decreases 0.74 (63.87%) for the rotational speed $\omega$ of 2000 r/min and 0.90 (77.94%) for the rotational speed $\omega$ of 3000 r/min. This is because with the further increase of the rotational speed $\omega$, the eccentricity ratio becomes smaller by the further enhanced hydrodynamic effect, which reduces sensitivity to change in fluid film thickness and decreases the averaging coefficients $\delta_x$ and $\delta_y$.

The radius clearance of the bearing $c$ as an important design parameter also affects the error averaging effect.

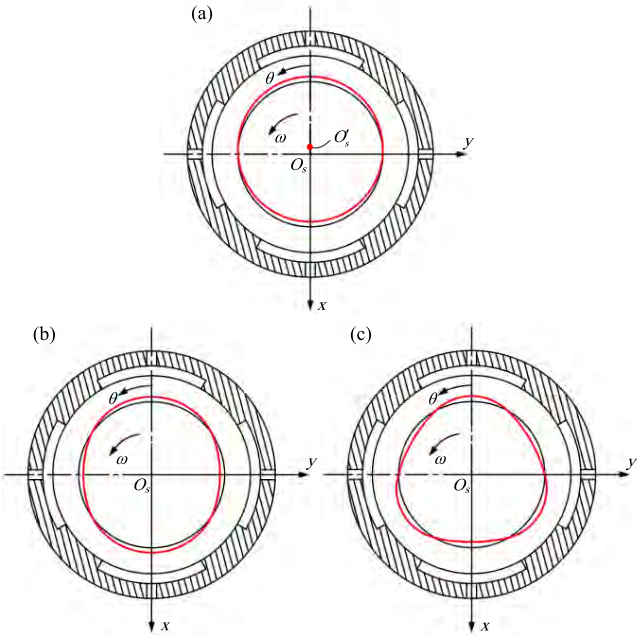


**FIGURE 8.** Roundness error of the shaft under different wave numbers $n$: (a) $n = 1$, (b) $n = 2$, and (c) $n = 3$.

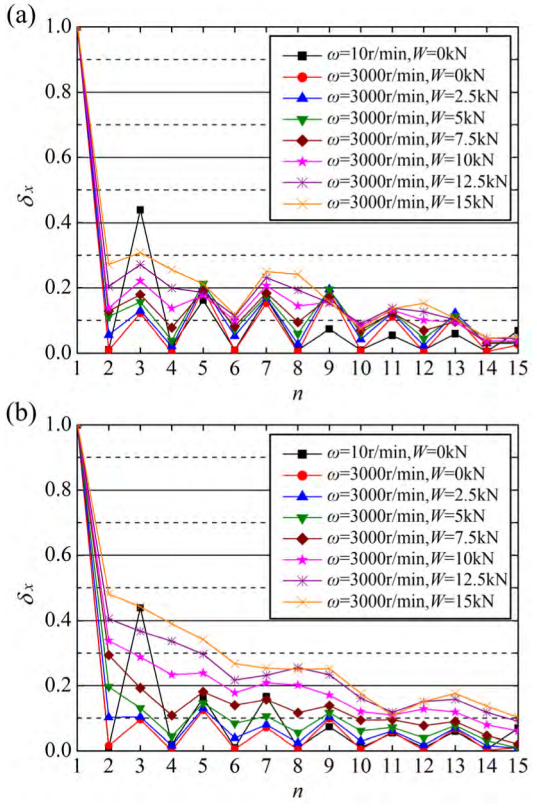


**FIGURE 9.** Averaging coefficients $\delta_x$ for different radius clearances $c$ and external loads $W$: (a) $c = 0.020$ mm, and (b) $c = 0.030$ mm.

The results in Figs. 6 and 7 are calculated under the radius clearance $c$ of 0.025 mm. As comparison, Figs. 9 and 10 show the variation of the averaging coefficients $\delta_x$ and $\delta_y$ with

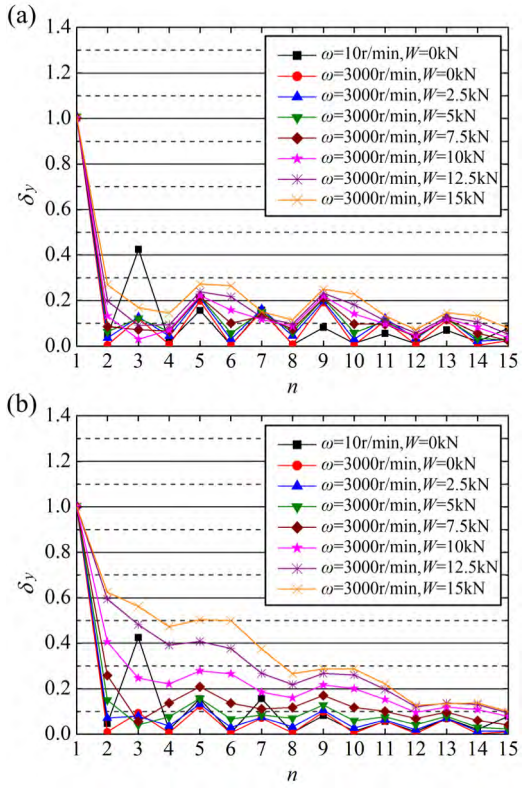


**FIGURE 10.** Averaging coefficients $\delta_y$ for different radius clearances $c$ and external loads $W$: (a) $c = 0.020$ mm, and (b) $c = 0.030$ mm.

the wave number $n$ for different radius clearances $c$ under rotational speeds $\omega$ of 3000 r/min, respectively.

By comparison of the results in Figs. 6(c), 9(a) and 9(b) where the radius clearance $c$ equals 0.025 mm, 0.020 mm and 0.030 mm, respectively, it is found that with the increase of the radius clearance $c$, the averaging coefficient $\delta_x$ is gradually increasing. As an example, under the wave number $n$ of 2 and the external load $W$ of 10 kN, relative to the case where the radius clearance $c$ of 0.020 mm, the averaging coefficient $\delta_x$ increases 0.1 (73.37%) for the radius clearance c of 0.025 mm and 0.2 (145.13%) for the radius clearance $c$ of 0.030 mm. By comparison of the results in Figs. 7(c), 10(a) and 10(b), it is found that the averaging coefficient $\delta_y$ has the same trend as the averaging coefficient $\delta_x$.

The change trend of the averaging coefficients can be further explained by the change of the transient orbit of the shaft, which also reflects the motion accuracy of the shaft. The transient orbit is analyzed in the following section.

### B. TRANSIENT ORBIT OF THE SHAFT

Figs. 11 and 12 show the variation of the transient orbit of the shaft for different rotational speeds $\omega$ and external loads $W$ under the wave number $n$ of 2 and 3, respectively. The original position of shaft orbit is freely set, which has no effect on the final shape of the transient orbit. It can be seen from Figs. 11 and 12 that:

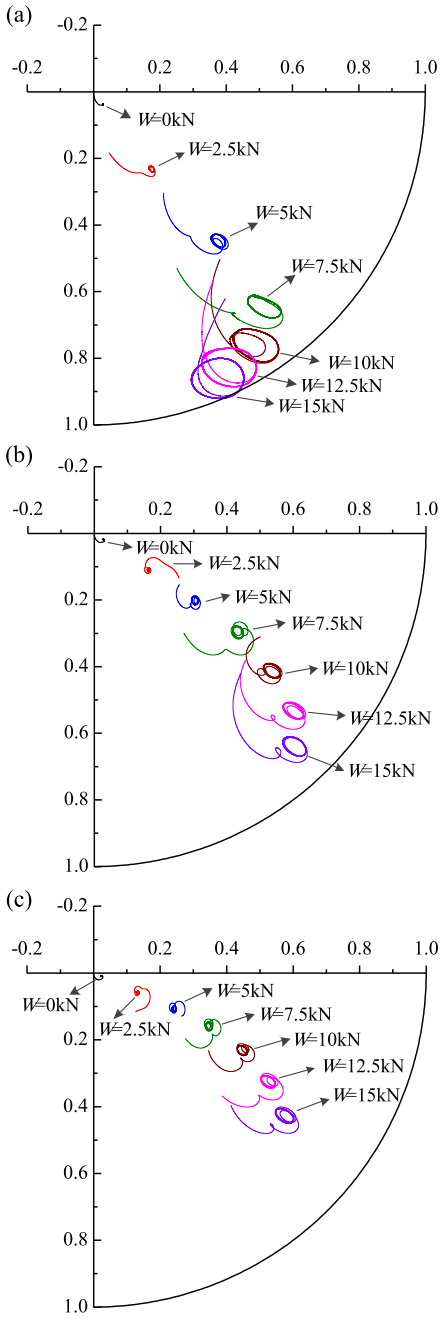


**FIGURE 11.** Transient orbit of the shaft under the wave number $n$ of 2 for different rotational speeds $\omega$ and external loads $W$: (a) $\omega$ = 1000 r/min, (b) $\omega$ = 2000 r/min, and (c) $\omega$ = 3000 r/min.

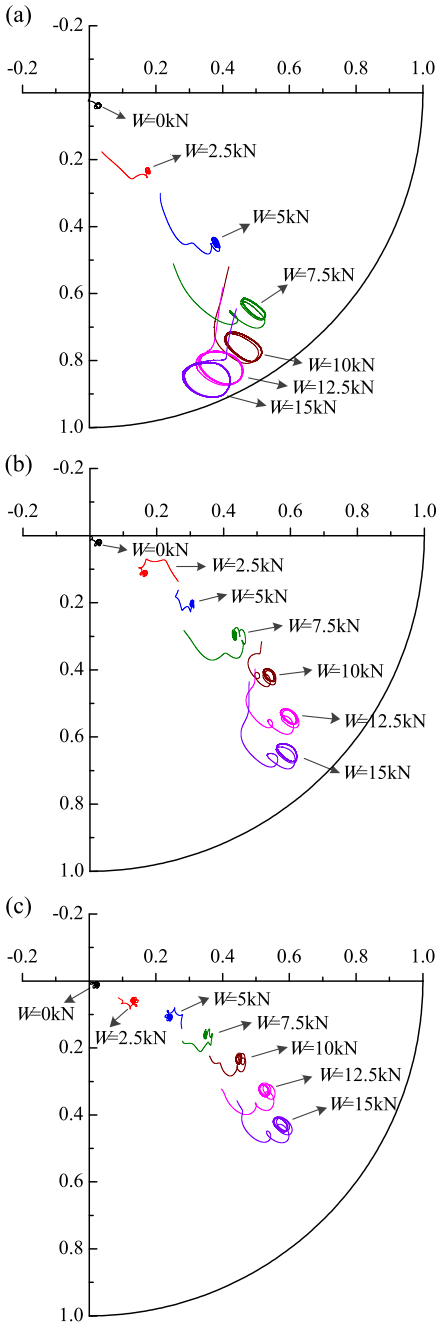


**FIGURE 12.** Transient orbit of the shaft under the wave number $n$ of 3 for different rotational speeds $\omega$ and external loads $W$: (a) $\omega$ = 1000 r/min, (b) $\omega$ = 2000 r/min, and (c) $\omega$ = 3000 r/min.

(1) The final shape of the transient orbit can be approximately regarded as an ellipse. With increase in the external load $W$ at any speeds, the center of the ellipse gradually moves away from the center of the bearing (the eccentricity ratio gradually increases) and the size of the ellipse is gradually increasing. Taking the Fig. 11(b) as an example, under the wave number $n$ of 2 and the rotational speed $\omega$ of 2000 r/min, the eccentricity ratios are 0.03, 0.20, 0.36, 0.52, 0.67, 0.80, and 0.88, and the long radiuses of the ellipse are 0.03 $\mu$m, 0.17 $\mu$m, 0.33 $\mu$m, 0.51 $\mu$m, 0.75 $\mu$m, 0.89 $\mu$m, and 0.99 $\mu$m for the external load $W$ increasing from 0 kN to 2.5 kN, 5 kN, 7.5 kN, 10 kN, 12.5 kN, and 15 kN, respectively. The increase of the size of the ellipse represents the radial motion errors increasing. Thus, the averaging coefficients $\delta_x$ and $\delta_y$ increase with increasing magnitude of the external loads $W$, as shown in Figs. 6 and 7.

(2) With the rotational speed $\omega$ increasing from 1000 r/min to 2000 r/min and 3000 r/min, the eccentricity ratio gradually decreases and the size of the ellipse is also gradually decreasing. As an example, in Figs. 11(a)-(c), under the wave

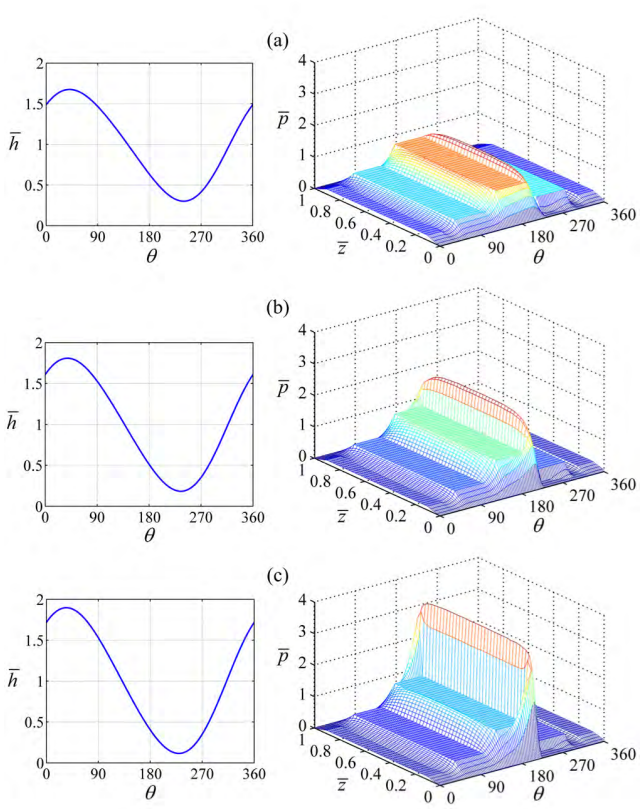


**FIGURE 13.** Fluid film thickness and pressure distribution under the rotational speed $\omega$ of 2000 r/min, the rotational angle of the shaft of 270° and the wave number $n$ of 2 for different external loads $W$: (a) $W = 10$ kN, (b) $W = 12.5$ kN, and (c) $W = 15$ kN.

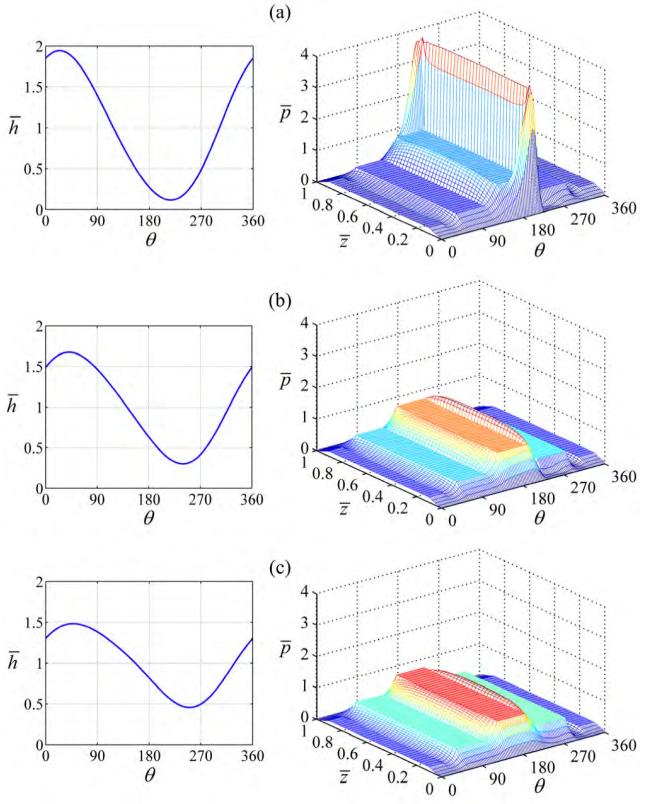


**FIGURE 14.** Fluid film thickness and pressure distribution under the external load $W$ of 10 kN, the rotational angle of the shaft of 270° and the wave number $n$ of 2 for different rotational speeds $\omega$: (a) $\omega = 1000$ r/min, (b) $\omega = 2000$ r/min, and (c) $\omega = 3000$ r/min.

number $n$ of 2 and the external load $W$ of 10 kN, the eccentricity ratios are 0.90, 0.67, and 0.50, and the long radiuses of the ellipse are 1.94 $\mu$m, 0.74 $\mu$m, and 0.45 $\mu$m for the rotational speed $\omega$ increasing from 1000 r/min to 2000 r/min and 3000 r/min, respectively. This demonstrates that the enhancing hydrodynamic force and squeeze film force can decrease the eccentricity ratio and improve the error averaging effect.

The internal factor of variation of ellipse orbits is based on the change of the pressure distribution with the rotation of the shaft and the resulting change of fluid film forces.

Fig. 13 depicts the fluid film thickness and pressure distribution for different external loads $W$ under the rotational speed $\omega$ of 2000 r/min and the rotational angle of the shaft of 270°. It is found that the pressure peaks appear near the smaller film thicknesses due to the hydrodynamic effect and squeeze film effect. The hydrodynamic pressure gradually increases with increasing magnitude of the external loads $W$. Fig. 14 depicts the fluid film thickness and pressure distribution for different rotational speeds $\omega$ under the external load $W$ of 10 kN and the rotational angle of the shaft of 270°. It can be seen that the hydrodynamic pressure gradually decreases with increasing rotational speed $\omega$, because the enhancing hydrodynamic force and squeeze film force decrease the eccentricity ratio of the shaft and increase the fluid film thickness.

Fig. 15 shows the variation of the fluid film forces with the rotation of the shaft under the rotational speed $\omega$ of 3000 r/min and the wave number $n$ of 2, when the shaft rotates keeping the shaft center located at the center of the ellipse. It is found that the fluid film forces fluctuate with the rotation of the shaft, which results in the variation of the position of the shaft center and generating the radial motion errors. With increase in the external loads $W$, the amplitude of the fluid film forces $\bar{F}_x$ and $\bar{F}_y$ gradually increase, which leads to the radial motion errors in the $x$ and $y$ directions increase, respectively. Fig. 16 shows the case of the change of the fluid film force $\bar{F}_y$ where the wave number $n$ equals 3. It can be seen that when the external loads $W$ increasing from 5 kN to 10 kN, the fluctuation of the fluid film force $\bar{F}_y$ presents reverse (the difference of the phase approximately equals half of a wavelength). The fluid film force $\bar{F}_y$ is in the phase reverse stage under the external loads $W$ of 7.5 kN, and thus the amplitude of the fluid film force $\bar{F}_y$ and the averaging coefficient $\delta_y$ are smaller in this case, as shown in Fig. 7(c).

### C. DISCUSSION ON ACCURACY DESIGN OF HYDROSTATIC JOURNAL BEARING

It is concluded from the above analysis, the rotational speed $\omega$, the external load $W$ and the wave number $n$ have significant influences on the error averaging effect of the

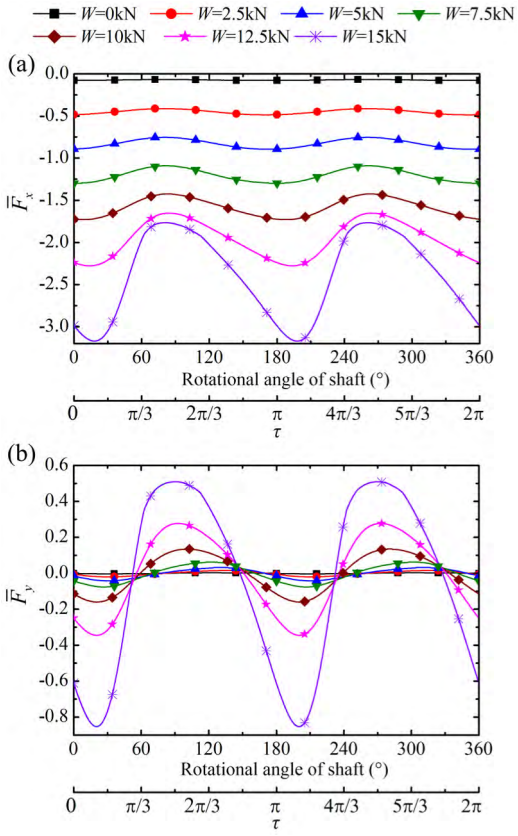


**FIGURE 15.** (a) Variation of fluid film forces $\bar{F}_x$ with the rotation of the shaft and (b) variation of fluid film forces $\bar{F}_y$ with the rotation of the shaft, under the rotational speed $\omega$ of 3000 r/min and the wave number $n$ of 2.

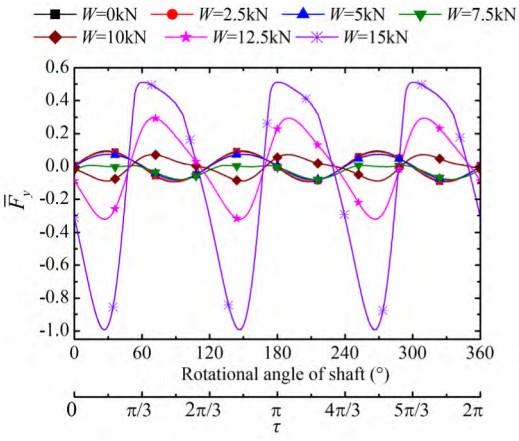


**FIGURE 16.** Variation of fluid film forces $\bar{F}_y$ with the rotation of the shaft, under the rotational speed $\omega$ of 3000 r/min and the wave number n of 3.

hydrostatic journal bearing, which should be comprehensively considered in the accuracy design phase.

The hydrostatic journal bearing often runs at different speeds and bears different external loads in precision applications. For no-load and low-speed condition [$W = 0$ kN and $\omega = 10$ r/min (quasi-static condition)], the radial motion error has a peak value at the wave number $n$ of 3, which should be avoided by changing the value of wave number $n$ through reprocessing the shaft or changing the working condition of low-speed to high-speed (reaches to 1000 r/min). For lower external load condition ($W \leq 5$ kN), the wave number $n$ should be tried to take an even number where the hydrostatic journal bearing has smaller averaging coefficients and higher motion accuracy. For higher external load condition ($W \geq 7.5$ kN), It is necessary to take a larger value for the rotational speed $\omega$ (reaches to 2000 r/min). As a whole, the motion accuracy of the shaft has an increasing trend with the increase of the wave number $n$ and the rotational speed $\omega$. When the wave number $n$ is larger than 9, the averaging coefficients $\delta_x$ and $\delta_y$ both have smaller values even under heavy-load condition. With increasing rotational speed $\omega$, the averaging coefficients $\delta_x$ and $\delta_y$ both gradually decrease under any external load.

## IV. CONCLUSIONS

A new mathematical model is presented for making a more realistic prediction of radial motion errors of the hydrostatic journal bearing, which including the influence of rotational speed of the shaft and the external load. The averaging coefficients, used for quantitatively measuring the error averaging effect of fluid film, are examined. And the transient orbits of the shaft are analyzed for further investigating the radial motion errors. The main conclusions are drawn as follows:

(1) Under no-load and low-speed (quasi-static) condition, the averaging coefficients $\delta_x$ and $\delta_y$ are both equal to zero (the shaft has no radial motion error) when the wave number $n$ equals an even number and are not zero when the wave number $n$ equals an odd number. As a whole, the averaging coefficients $\delta_x$ and $\delta_y$ have a decreasing trend with increasing wave number $n$. And under the wave number $n$ of 3, the averaging coefficients $\delta_x$ and $\delta_y$ have a larger value.

(2) Under no-load condition, with the rotational speed $\omega$ increasing from 0 r/min to 1000 r/min, the averaging coefficients $\delta_x$ and $\delta_y$ have an obvious decrease. With the external load $W$ increasing from 0 kN to a smaller value ($W \leq 5$ kN), the averaging coefficients $\delta_x$ and $\delta_y$ are gradually increasing and become not equal to zero for even number of wave. With the external load $W$ further increasing to a larger value ($7.5\text{ kN} \leq W \leq 15\text{ kN}$), the error averaging effect deteriorates significantly.

(3) With the rotational speed $\omega$ increasing from 1000 r/min to 2000 r/min and 3000 r/min, the averaging coefficients $\delta_x$ and $\delta_y$ have an obvious decrease, because the enhanced hydrodynamic effect decreases the eccentricity ratio and reduces sensitivity to the roundness errors of the shaft.

(4) The final shape of the transient orbit of the shaft can be approximately regarded as an ellipse. With increase in the external load $W$, the center of the ellipse gradually moves away from the center of the bearing and the size of the ellipse is gradually increasing. With increase in the rotational speed $\omega$, the eccentricity ratio gradually decreases and the size of the ellipse is also gradually decreasing.

## NOMENCLATURE

$a_b$ = bearing land width in axial direction, mm
$c$ = radial clearance, mm
$c_h$ = specific heat capacity of lubricant, J/(kg °C)
$D$ = shaft diameter, mm
$d_c$ = diameter of capillary restrictor, mm
$d_r$ = depth of recess, mm
$E$ = amplitude of the roundness error of the shaft, mm
$E_l$ = apparent bulk modulus of the lubricant, Pa
$E_c$ = bulk modulus of the connected channel, Pa
$e$ = eccentricity, mm
$F_x$ = fluid film force in the $x$ direction, N
$F_y$ = fluid film force in the $y$ direction, N
$F_f$ = frictional force, N
$h$ = fluid film thickness, mm
$L$ = bearing length, mm
$L_r$ = recess length, mm
$l_c$ = length of capillary restrictor, mm
$M$ = mass of the shaft, kg
$n$ = wave number of roundness errors
$O_b$ = bearing center
$O_s$ = shaft center
$oxyz$ = Cartesian coordinates
$p$ = pressure, Pa
$p_s$ = supply pressure, Pa
$p_{rk}$ = $k$th recess pressure, Pa
$p_p$ = input power of oil pump, kW
$p_f$ = friction power, kW
$Q_{ck}$ = flow through the $k$th capillary restrictor, mm$^3$/s
$Q_{ink}$ = flow entering the $k$th recess land, mm$^3$/s
$Q_s$ = total flow, mm$^3$/s
$r$ = shaft radius, mm
$t$ = time, s
$T$ = temperature, °C
$V_{ck}$ = connected channel volume, mm$^3$
$V_{rk}$ = $k$th recess volume, mm$^3$
$v$ = velocity on outer cylinder of shaft, m/s
$W$ = external load, N
$x_s$, $y_s$ = coordinates of shaft center
$\dot{x}_s$ = speed of shaft in $x$ direction, mm/s
$\ddot{x}_s$ = acceleration of shaft in $x$ direction, mm/s$^2$
$\dot{y}_s$ = speed of shaft in $y$ direction, mm/s
$\ddot{y}_s$ = acceleration of shaft in $y$ direction, mm/s$^2$

## GREEK SYMBOLS

$\beta$ = viscosity-temperature index
$\delta_x$ = averaging coefficient in $x$ direction
$\delta_y$ = averaging coefficient in $y$ direction
$\eta$ = dynamic viscosity of lubricant, Pa s
$\theta$ = angular coordinate
$\theta_r$ = wrap angle of recess
$\rho$ = density of lubricant, kg/m$^3$
$\phi$ = attitude angle
$\varphi$ = phase of the roundness error of the shaft
$\omega$ = rotational speed of shaft, r/min

## NON-DIMENSIONAL PARAMETERS

$\bar{C}_{sr} = 3\pi d_c^4/\left(32c^3 l_c\right)$
$\bar{E} = E/c$
$\bar{F}_x = F_x/(p_s L r)$
$\bar{F}_y = F_y/(p_s L r)$
$\bar{h} = h/c$
$\bar{p} = p/p_s$
$\bar{p}_{rk} = p_{rk}/p_s$
$\bar{Q} = \left(12\eta/p_s c^3\right) Q$
$\bar{Q}_{ck} = \left(12\eta/(p_s c^3)\right) Q_{ck}$
$\bar{Q}_{ink} = \left(12\eta/(p_s c^3)\right) Q_{ink}$
$\bar{V}_k = \dot{V}_k/(cr\omega L)$
$\overline{W}_x = W_x/(p_s L r)$
$\overline{W}_y = W_y/(p_s L r)$
$\bar{x}_s = \varepsilon\cos\phi$
$\bar{\dot{x}}_s = \dot{x}_s/(c\omega)$
$\bar{\ddot{x}}_s = \ddot{x}_s/(c\omega^2)$
$\bar{y}_s = \varepsilon\sin\phi$
$\bar{\dot{y}}_s = \dot{y}_s/(c\omega)$
$\bar{\ddot{y}}_s = \ddot{y}_s/(c\omega^2)$
$\bar{z} = z/L$
$\varepsilon = e/c$
$\tau = \omega t$
$\Lambda = 6\eta\omega r^2/(p_s c^2)$
$\Lambda_2 = 12\eta\omega V_k/\left(c^3 E_l\right)$
$\Lambda_3 = p_s L r/(Mc\omega^2)$
$\Lambda_4 = g/(c\omega^2)$

## SUBSCRIPTS AND SUPERSCRIPTS

$b$ = bearing
$c$ = capillary
$r$ = recess
$s$ = shaft or supply
$x$ = in $x$ direction
$y$ = in $y$ direction
$\bar{\ }$ = corresponding non-dimensional parameter

## REFERENCES

[1] Z. F. Liu, Y. M. Wang, L. G. Cai, Y. Zhao, Q. Cheng, and X. Dong, "A review of hydrostatic bearing system: Researches and applications," *Adv. Mech. Eng.*, vol. 9, no. 10, pp. 1–27, 2017.

[2] N. R. Kane, J. Sihler, and A. H. Slocum, "A hydrostatic rotary bearing with angled surface self-compensation," *Precis. Eng.*, vol. 27, no. 2, pp. 125–139, 2003.

[3] M. Aleyaasin, R. Whalley, and M. Ebrahimi, "Error correction in hydrostatic spindles by optimal bearing tuning," *Int. J. Mach. Tools Manuf.*, vol. 40, no. 6, pp. 809–822, 2000.

[4] S. Cappa, D. Reynaerts, and F. Al-Bender, "Reducing the radial error motion of an aerostatic journal bearing to a nanometre level: Theoretical modelling," *Tribol. Lett.*, vol. 53, no. 1, pp. 27–41, 2014.

[5] G. Jang and S.-W. Jeong, "Vibration analysis of a rotating system due to the effect of ball bearing waviness," *J. Sound Vib.*, vol. 269, nos. 3–5, pp. 709–726, 2004.

[6] P. Zhang, Y. L. Chen, and J. Zha, "Relationship between geometric errors of thrust plates and error motions of hydrostatic thrust bearings under quasi-static condition," *Precis. Eng.*, vol. 50, pp. 119–131, Oct. 2017.

[7] P. Zhang, Y. Chen, and X. Liu, "Relationship between roundness errors of shaft and radial error motions of hydrostatic journal bearings under quasi-static condition," *Precis. Eng.*, vol. 51, pp. 564–576, Jan. 2018.

[8] H. Cui, Y. Wang, X. Yue, M. Huang, W. Wang, and Z. Jiang, "Numerical analysis and experimental investigation into the effects of manufacturing errors on the running accuracy of the aerostatic porous spindle," *Tribol. Int.*, vol. 118, nos. 20–36, Feb. 2018.
[9] E. Shamoto, C.-H. Park, and T. Moriwaki, "Analysis and improvement of motion accuracy of hydrostatic feed table," *CIRP Ann.*, vol. 50, no. 1, pp. 285–290, 2001.
[10] T. O. Ekinci and J. R. R. Mayer, "Relationships between straightness and angular kinematic errors in machines," *Int. J. Mach. Tools Manuf.*, vol. 47, nos. 12–13, pp. 1997–2004, 2007.
[11] T. O. Ekinci, J. R. R. Mayer, and G. M. Cloutier, "Investigation of accuracy of aerostatic guideways," *Int. J. Mach. Tools Manuf.*, vol. 49, no. 6, pp. 478–487, 2009.
[12] F. Xue, W. Zhao, Y. Chen, and Z. Wang, "Research on error averaging effect of hydrostatic guideways," *Precis. Eng.*, vol. 36, no. 1, pp. 84–90, 2012.
[13] J. Zha, D. Lv, Q. Jia, and Y. Chen, "Motion straightness of hydrostatic guideways considering the ratio of pad center spacing to guide rail profile error wavelength," *Int. J. Adv. Manuf. Technol.*, vol. 82, nos. 9–12, pp. 2065–2073, 2016.
[14] J. Zha, Y. Chen, and Z. Wang, "A tolerance design method for hydrostatic guideways motion accuracy based on error averaging effect," *Procedia CIRP*, vol. 75, pp. 196–201, Jan. 2018.
[15] E. Qi, Z. Fang, T. Sun, J. Chen, C. Liu, and J. Wang, "A method for predicting hydrostatic guide error averaging effects based on three-dimensional profile error," *Tribol. Int.*, vol. 95, pp. 279–289, Mar. 2011.
[16] Y. Zhang, C. Lu, W. Pan, S. Chen, and Z. Liu, "Averaging effect on pitch errors in hydrostatic lead screws with continuous helical recesses," *J. Tribol.*, vol. 138, no. 2, 2016, Art. no. 021103.
[17] Y. Zhang, C. Lu, W. Pan, S. Chen, and Y. Liu, "Transient motion of hydrostatic lead screws with continuous helical recesses," *J. Tribol.*, vol. 139, no. 1, 2017, Art. no. 011703.
[18] P. Zhang, Y. Chen, C. Zhang, J. Zha, and T. Wang, "Influence of geometric errors of guide rails and table on motion errors of hydrostatic guideways under quasi-static condition," *Int. J. Mach. Tools Manuf.*, vol. 125, pp. 55–67, Feb. 2018.
[19] G. He, G. Sun, H. Zhang, C. Huang, and D. Zhang, "Hierarchical error model to estimate motion error of linear motion bearing table," *Int. J. Adv. Manuf. Technol.*, vol. 93, nos. 5–8, pp. 1915–1927, 2017.
[20] G. Khim, J. S. Oh, and C. H. Park, "Analysis of 5-DOF motion errors influenced by the guide rails of an aerostatic linear motion stage," *Int. J. Precis. Eng. Manuf.*, vol. 15, no. 2, pp. 283–290, 2014.
[21] G. Khim, C. H. Park, E. Shamoto, and S. W. Kim, "Prediction and compensation of motion accuracy in a linear motion bearing table," *Precis. Eng.*, vol. 35, no. 3, pp. 393–399, 2011.
[22] H. Tang, J.-A. Duan, and Q. Zhao, "A systematic approach on analyzing the relationship between straightness & angular errors and guideway surface in precise linear stage," *Int. J. Mach. Tools Manuf.*, vol. 120, pp. 12–19, Sep. 2017.
[23] Z. Wang, W. Zhao, Y. Chen, and B. Lu, "Prediction of the effect of speed on motion errors in hydrostatic guideways," *Int. J. Mach. Tools Manuf.*, vol. 64, pp. 78–84, Jan. 2013.
[24] J. Zha, Y. Chen, and P. Zhang, "Precision design of hydrostatic thrust bearing in rotary table and spindle," *Proc. Inst. Mech. Eng., B, J. Eng. Manuf.*, vol. 232, no. 11, pp. 2044–2053, 2018.
[25] R. G. Kirk and E. J. Gunter, "Short bearing analysis applied to rotor dynamics—Part 2: Results of journal bearing response," *J. Lubrication Technol.*, vol. 98, no. 2, pp. 319–329, 1976.
[26] P. Liang, C. Lu, J. Ding, and S. Chen, "A method for measuring the hydrodynamic effect on the bearing land," *Tribol. Int.*, vol. 67, pp. 146–153, Nov. 2013.

**YONGTAO ZHANG** received the Ph.D. degree in mechatronic engineering from Shandong University, Jinan, in 2017. Then, he joined the College of Electromechanical Engineering, Qingdao University of Science and Technology, Qingdao, China, as a Lecturer. His current research interests include the electromechanical drive, friction, and lubrication.

**CHANGHOU LU** received the B.E., M.S., and Ph.D. degrees from Shandong University, Jinan, China, in 1983, 1988, and 1996, respectively. He is currently a Professor with Shandong University. His research interests are electromechanical drive, sophisticated detection technology of electromechanical systems, hydrodynamic lubrication, hydrostatic lubrication, friction, and wear.

**HAIXIA ZHAO** received the B.S. degree in mechanical engineering from Xi'an Shiyou University, Xi'an, China, in 1991, and the M.S. degree in mechanical engineering from the Qingdao University of Science and Technology, Qingdao, China, in 2007, where she is currently pursuing the Ph.D. degree with the College of Electromechanical Engineering. In 2000, she joined the College of Electromechanical Engineering, Qingdao University of Science and Technology, where she has been an Assistant Professor, since 2008. Her research interests include mechanical design and material science.

**WEIJIE SHI** received the B.S. degree in mechanical engineering from the Wuhan University of Technology, Wuhan, China, in 2012, and the Ph.D. degree in mechanical engineering from the Huazhong University of Science and Technology, Wuhan, in 2018. Then, he joined the College of Electromechanical Engineering, Qingdao University of Science and Technology, Qingdao, China, as a Lecturer. His current research interests include the material design of water hydraulics components and computational materials science.

**PENG LIANG** received the B.S. degree in mechanical engineering from the Qingdao University of Technology, Qingdao, China, in 2009, and the Ph.D. degree in mechatronic engineering from Shandong University, Jinan, in 2014. Then, he joined the School of Mechanical and Automotive Engineering, Qingdao University of Technology, Qingdao, as a Lecturer. He was rated as an Assistant Professor, in 2018. His current research interests include the electromechanical drive, friction, and lubrication.